

Polymorphism of Oligomers of a Peptide from β -Amyloid

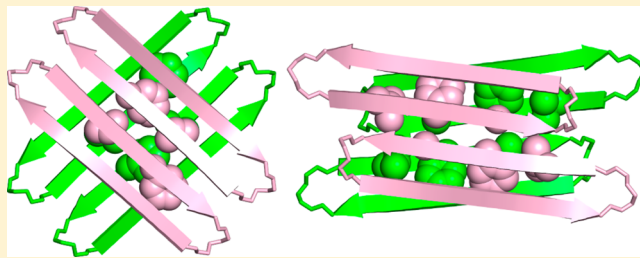
Johnny D. Pham,[†] Borries Demeler,[‡] and James S. Nowick*,[†]

[†]Department of Chemistry, University of California, Irvine, Irvine, California 92697-2025, United States

[‡]Department of Biochemistry, University of Texas Health Science Center, San Antonio, Texas 78229-3900, United States

S Supporting Information

ABSTRACT: This contribution reports solution-phase structural studies of oligomers of a family of peptides derived from the β -amyloid peptide ($A\beta$). We had previously reported the X-ray crystallographic structures of the oligomers and oligomer assemblies formed in the solid state by a macrocyclic β -sheet peptide containing the $A\beta_{15-23}$ nonapeptide. In the current study, we set out to determine its assembly in aqueous solution. In the solid state, macrocyclic β -sheet peptide **1** assembles to form hydrogen-bonded dimers that further assemble in a sandwich-like fashion to form tetramers through hydrophobic interactions between the faces bearing V_{18} and F_{20} . In aqueous solution, macrocyclic β -sheet peptide **1** and homologue **2a** form hydrogen-bonded dimers that assemble to form tetramers through hydrophobic interactions between the faces bearing L_{17} , F_{19} , and A_{21} . In the solid state, the hydrogen-bonded dimers are antiparallel, and the β -strands are fully aligned, with residues 17–23 of one of the macrocycles aligned with residues 23–17 of the other. In solution, residues 17–23 of the hydrogen-bonded dimers are shifted out of alignment by two residues toward the C-termini. The two hydrogen-bonded dimers are nearly orthogonal in the solid state, while in solution the dimers are only slightly rotated. The differing morphology of the solution-state and solid-state tetramers is significant, because it may provide a glimpse into some of the structural bases for polymorphism among $A\beta$ oligomers in Alzheimer's disease.



INTRODUCTION

Soluble amyloid oligomers are now thought to be the main toxic species that cause neurodegeneration in Alzheimer's and other amyloid diseases.^{1–10} Small assemblies made up of dimers, trimers, and tetramers of the β -amyloid peptide ($A\beta$), as well as larger assemblies such as dodecamers, have been shown to disrupt synaptic activity and cause neuronal cell death.^{11–17} Atomic-level details of the structures of amyloid oligomers are desperately needed in order to understand how the oligomers form and the molecular basis by which they cause neurodegeneration.

The oligomers are polymorphic and dynamic, forming as different species and equilibrating slowly with the monomer and with β -amyloid fibrils, which are generally more stable.^{8,9,18–20} While the structures of amyloid oligomers are still largely unknown, a number of approaches have been taken to gain insights into their structures. β -Sheet structure and interactions—a common feature of amyloid fibril formation—are generally thought to be important in the structures and interactions of amyloid oligomers.^{20–25} Incorporation of amyloidogenic peptides into larger proteins can control amyloid supramolecular assembly and allow observation of oligomeric assemblies at atomic resolution.²⁶ Peptide fragments can also serve as chemical models of oligomers; X-ray crystallographic studies of these peptide fragments have provided insights into the structures of amyloid oligomers.^{27,28} Chemical cross-links within amyloidogenic monomers that stabilize folded β -sheet conformations can promote oligomer

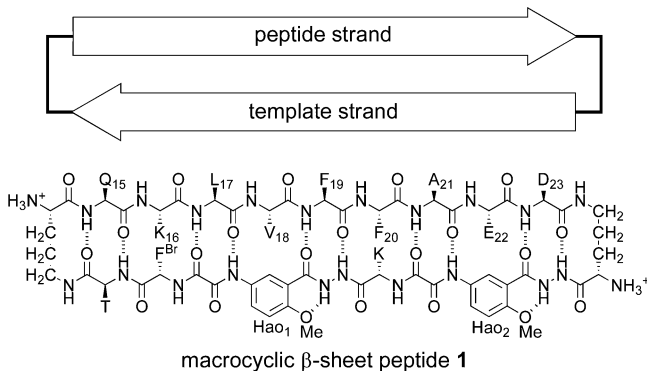
formation and help prevent fibril formation.^{29–31} These cross-linked systems are more amenable to study and can provide simpler and more stable chemical models of the unstable oligomers formed by amyloidogenic peptides and proteins. Computational models of oligomers have been constructed from atomic-level structures of amyloid fibrils, which are understood far better at atomic resolution than the oligomers.^{32–34}

Our laboratory is gaining insights into the structures and interactions of amyloid oligomers by combining fragments of amyloidogenic peptides and proteins with molecular templates to create macrocycles that promote β -sheet structure and interactions while blocking amyloid fibril formation.^{35,36} We recently reported the X-ray crystallographic structures of oligomers of a peptide from β -amyloid.³⁷ We incorporated the nonapeptide sequence QKLVFFAED ($A\beta_{15-23}$) into macrocyclic β -sheet peptide **1**, with δ -linked ornithine turn units and a template strand that features an unnatural amino acid, Hao.^{38,39} In the solid state, the macrocycle folds to form a β -sheet. The β -sheet forms a hydrogen-bonded dimer, which assembles face-to-face to make a cruciform tetramer, which is a key subunit of the lattice. The cruciform tetramers assemble into triangular dodecamers, and the triangular dodecamers further assemble into the lattice.

Received: January 28, 2014

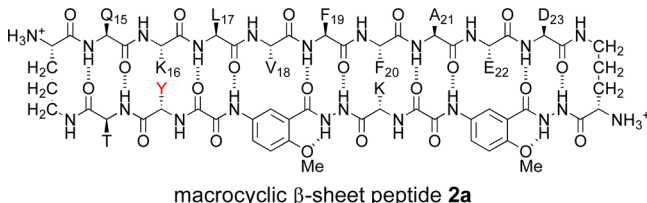
Published: March 26, 2014





The hydrogen-bonded dimers are antiparallel, and the β -strands are fully aligned, with residues 17–23 of one of the macrocycles aligned with residues 23–17 of the other. The resulting four-stranded β -sheet forms a plane, with the side chains projecting from the upper and lower faces of the plane. Residues K₁₆, V₁₈, F₂₀, and E₂₂ of each macrocycle project from one face of the plane (the VF face), and residues Q₁₅, L₁₇, F₁₉, A₂₁, D₂₃ of each macrocycle project from the other face of the plane (the LFA face). The VF face has the hydrophobic residues V₁₈ and F₂₀ flanked by the polar residues K₁₆ and E₂₂. The LFA face has the hydrophobic residues L₁₇, F₁₉, and A₂₁ flanked by the polar residues Q₁₅ and D₂₃. The hydrogen-bonded dimers assemble in a crisscross fashion through hydrophobic interactions between the VF faces to give the cruciform tetramers. Figure 1 illustrates the faces of the macrocycle and the structure of the cruciform tetramer.

In the current study, we set out to determine how macrocyclic β -sheet peptides containing the $\text{A}\beta_{15-23}$ nonapeptide assemble in solution. We began by using ¹H NMR spectroscopy to study how macrocyclic β -sheet peptide 2a folds and oligomerizes in aqueous solution. We had envisioned macrocyclic β -sheet 1 as a homologue of macrocyclic β -sheet 2a. The two molecules differ only in that 1 contains a *p*-bromophenylalanine (F^{BBr}) in the template strand, for single anomalous dispersion (SAD) phasing in X-ray crystallographic structure determination, while 2a contains a tyrosine.³⁷ As our studies of macrocyclic β -sheet 2a unfolded, we prepared additional homologues (2b, 2c, 3, and 4) to interrogate the assembly process. The following describes these studies and elucidates how the tetramer that forms in solution differs from that which forms in the solid state.



RESULTS

1. Tetramerization of Macrocylic β -Sheet Peptides 1 and 2a. We investigated the folding and assembly of the macrocyclic β -sheets in D₂O and in H₂O–D₂O solution by NMR spectroscopy. At millimolar concentrations, the ¹H NMR spectrum of macrocyclic β -sheet 2a is disperse, with methyl resonances from L₁₇ and A₂₁ unusually upfield (−0.35 and 0.49 ppm), aromatic resonances from F₁₉ unusually upfield (6.28 and 6.52 ppm), and many of the amino acid α -protons unusually downfield (\geq 5.0 ppm). One of the resonances from

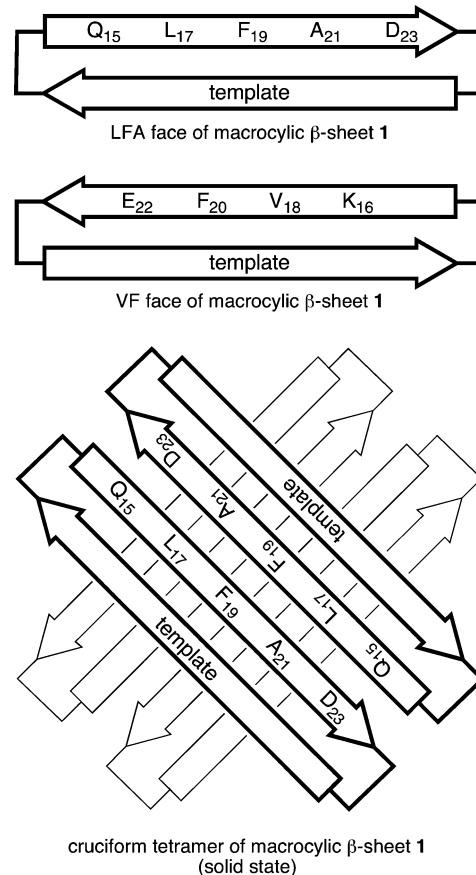


Figure 1. Cartoon illustrating the LFA and VF faces of macrocyclic β -sheet 1 and the cruciform tetramer formed in the solid state. The VF faces form the inner hydrophobic core of the cruciform tetramer, and the LFA faces form the outer surface.

one of the Hao amino acids (the H₄ resonance of H_{ao1}) appears unusually downfield at 9.17 ppm. The upfield shifting of the aromatic and aliphatic resonances is characteristic of the formation of an oligomer with a well-packed hydrophobic core comprising aromatic residues (Hao, Phe, etc.) and aliphatic residues (Leu, Ala, etc.). Minor additional resonances, associated with a monomer lacking a hydrophobic core are also present, most notably at 0.69–0.79 ppm (L₁₇ and V₁₈). Figure 2 illustrates the ¹H NMR spectrum of macrocyclic β -sheet 2a at 2.0 mM in D₂O solution.

The ¹H NMR spectrum of macrocyclic β -sheet 1 is virtually identical to that of macrocyclic β -sheet 2a, indicating that both peptides fold and oligomerize in a similar fashion in solution. The ¹H NMR spectrum of macrocyclic β -sheet 1 also exhibits additional minor resonances from L₁₇ and V₁₈ associated with a monomer lacking a hydrophobic core. These resonances are similar in intensity to those of macrocyclic β -sheet 2a, indicating that the oligomers formed by both macrocycles are similar in association constant (K_{assoc}) as well as in structure.

¹H NMR NOESY studies establish the formation of hydrogen-bonded dimers that are antiparallel, with the β -strands of residues 17–23 shifted out of alignment by two residues toward the C-termini (Figure 3). Notably, the NOESY spectrum in D₂O exhibits strong NOEs between the α -protons of L₁₇ and D₂₃ and between the α -protons of F₁₉ and A₂₁ (Figure 4). These NOEs reflect dimer formation. Additional strong NOEs associated with β -sheet folding of the macrocycles

1

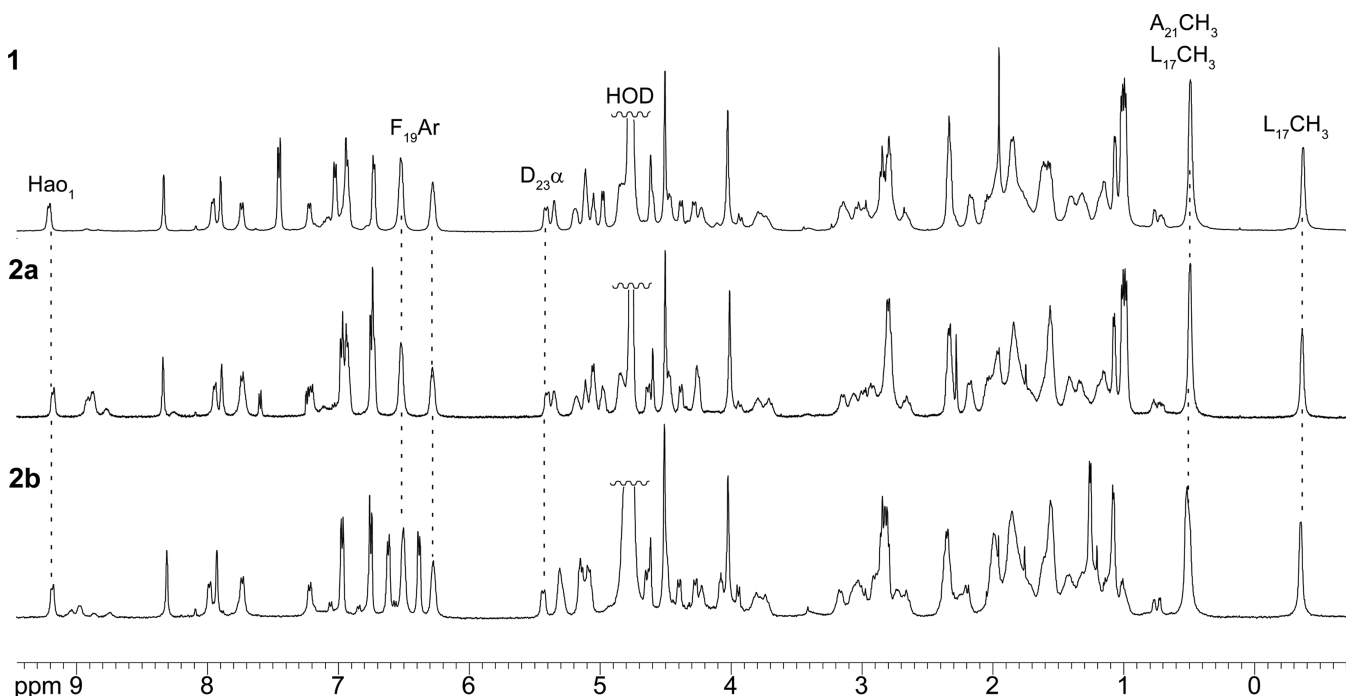


Figure 2. ^1H NMR spectra of macrocyclic β -sheet peptides **1**, **2a**, and **2b** at 2.0 mM in D_2O at 500 MHz and 298 K. Noteworthy resonances that reflect important shared features of the folding and assembly of these peptides are labeled and highlighted with dashed lines.

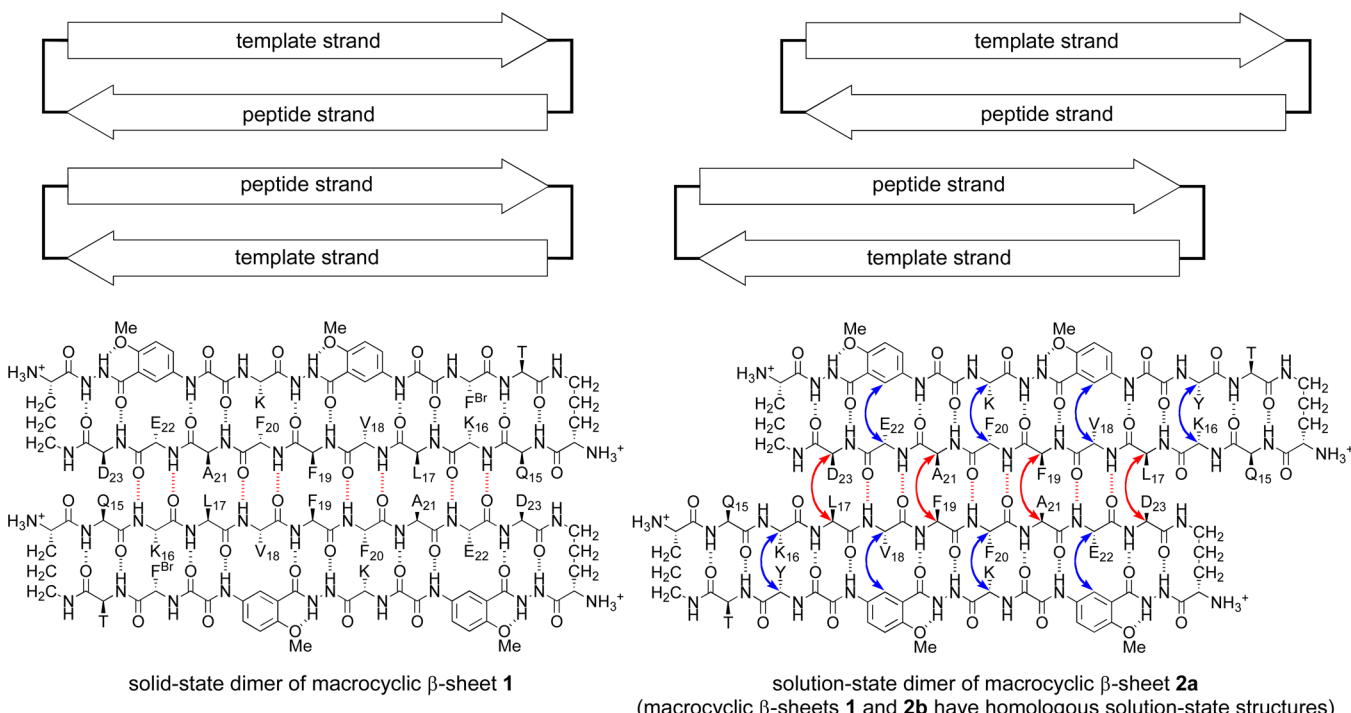


Figure 3. Cartoons and chemical structures illustrating the hydrogen-bonded dimers formed by macrocyclic β -sheet peptide **1** in the solid state (left) and by both macrocyclic β -sheet peptides **2a** and **1** in solution (right). Both hydrogen-bonded dimers are antiparallel: In the solid-state dimer, residues 17–23 of one of the macrocycles align with residues 23–17 of the other; in the solution-state dimers, these β -strands are shifted out of alignment by two residues toward the C-termini. Key NOEs associated with solution-state dimerization and folding of **2a** are shown with red and blue arrows.

occur between the α -protons of K_{16} and Y and between the α -protons of F_{20} and K (Figure 4). Other NOEs characteristic of folding are described in detail in the SI, as are additional NOEs associated with folding and dimerization that are seen in the NOESY spectrum in $\text{H}_2\text{O}-\text{D}_2\text{O}$ (90:10) (Figure S1a and b in

the SI). Macrocylic β -sheet **1** exhibits similar patterns of NOEs, indicating that it folds and dimerizes in a fashion similar to that of macrocycle **2a** (Figure S2 in the SI). The shifted structure of the dimers formed by the macrocycles in solution

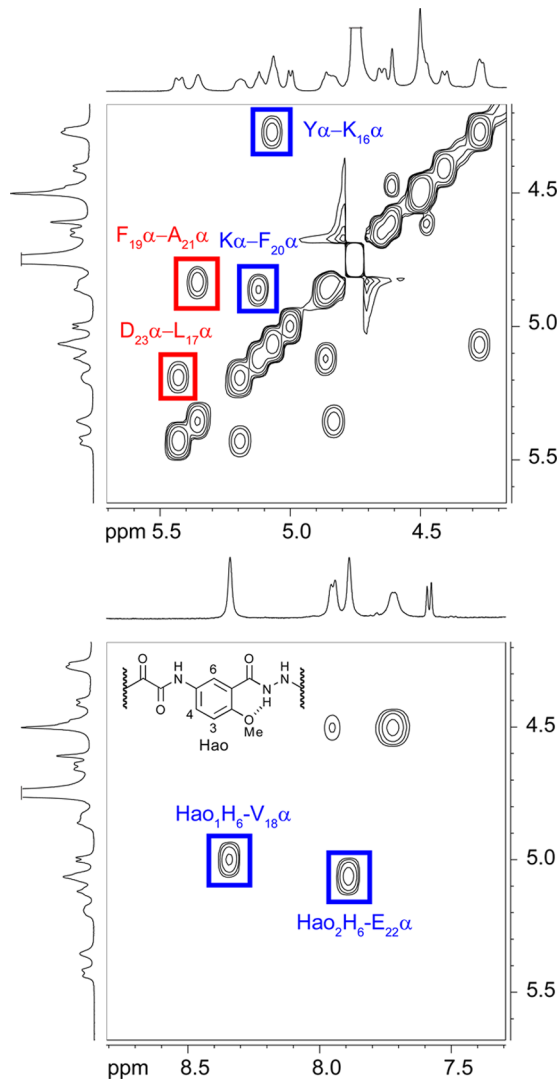


Figure 4. Selected expansions of the NOESY spectrum of macrocyclic β -sheet peptide **2a** at 8.0 mM in D_2O at 500 MHz and 300.5 K. Key intermolecular interstrand NOEs associated with dimerization are highlighted in red; key intramolecular interstrand NOEs associated with folding are highlighted in blue.

stands in sharp contrast to the aligned structure of macrocycle **1** in the solid state (Figure 3).

At low concentrations (e.g., ≤ 0.1 mM), the monomer predominates in the 1H NMR spectrum of macrocyclic β -sheet **2a**. The methyl resonances from L_{17} and V_{18} of the monomer are prominent at 0.69–0.79 ppm, and the methyl resonances from L_{17} and A_{21} of the oligomer at –0.35 and 0.49 ppm are small. As the concentration of **2a** is increased, the relative intensities of the resonances from the oligomer increase and the relative intensities of the resonances from the monomer decrease (Figure 5 and Figure S3 in the SI).⁴⁰ At 0.2 mM, the resonances of the monomer and oligomer are roughly equal in intensity.⁴¹ At high concentrations (e.g., 8.0 mM), the resonances of the monomer are barely visible. The strong concentration dependence of the monomer–oligomer equilibrium is not consistent with a simple monomer–dimer equilibrium, but rather reflects cooperative association in which the dimers are a subunit of a higher-order oligomer—in this case a tetramer consisting of a dimer of dimers.

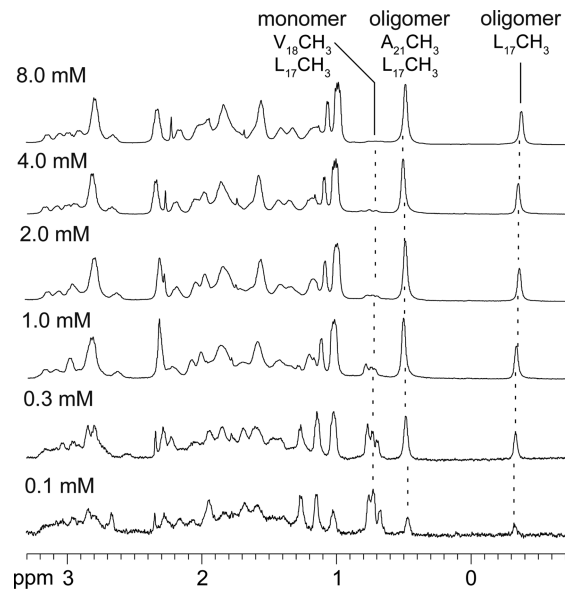


Figure 5. Expansions of the 1H NMR spectra of macrocyclic β -sheet peptide **2a** at various concentrations in D_2O at 500 MHz and 298 K. Noteworthy characteristic resonances of the monomer and the oligomer are labeled and highlighted with dashed lines.

The NOESY spectrum of macrocyclic β -sheet **2a** shows additional crosspeaks that are consistent with a tetramer in which two hydrogen-bonded dimers form a sandwich-like assembly. Notably, the NOESY spectrum in D_2O exhibits NOEs between Hao_2 and threonine and between Hao_2 and Hao_1 that only make sense as interlayer NOEs between the hydrogen-bonded dimers. Specifically, the methoxy group of Hao_2 gives NOEs with the methyl group of threonine, and the H_3 and H_4 protons of Hao_2 give NOEs with the H_3 and H_4 protons of Hao_1 . Figure 6 illustrates these interlayer NOE crosspeaks in the NOESY spectrum; Figure 7 illustrates the sandwich-like assembly consistent with these NOEs.⁴² Figure S4 and Table S1 (SI) provide additional data.

The four threonines of the tetramer point toward the interior of the sandwich-like assembly, as do all of the residues on the LFA faces of the β -sheets (Q_{15} , L_{17} , F_{19} , A_{21} , and D_{23}). The magnetic anisotropy from the packed aromatic groups of the resulting hydrophobic core shift the methyl resonances of L_{17} and A_{21} upfield. The magnetic anisotropy also shifts the aromatic ring protons of F_{19} upfield. Thus, the structure of this solution-state tetramer, in which the LFA faces make up the hydrophobic core, differs markedly from the structure of the solid-state tetramer, in which the VF faces make up the hydrophobic core. In the solid-state structure, the LFA faces are on the exterior of the tetramer and the VF faces are on the interior; in the solution-state structure, the VF faces are on the exterior and the LFA faces are on the interior.

2. Disruption of Tetramer Formation. To probe the assembly of the tetramer, we studied macrocyclic β -sheet peptide **3**. Macrocylic β -sheet **3** is a homologue of **2a** with a lysine in place of the threonine in the template strand. At 1.0 mM essentially no tetramer is observed in the 1H NMR spectrum of **3** (Figure 8). As the concentration is increased to 2.0 and 4.0 mM, resonances for the tetramer appear; at 8.0 mM the tetramer predominates. The tetramerization is far weaker than that of macrocyclic β -sheet **2a**, in which the tetramer is observed at 0.1 mM and predominates at 0.3 mM.

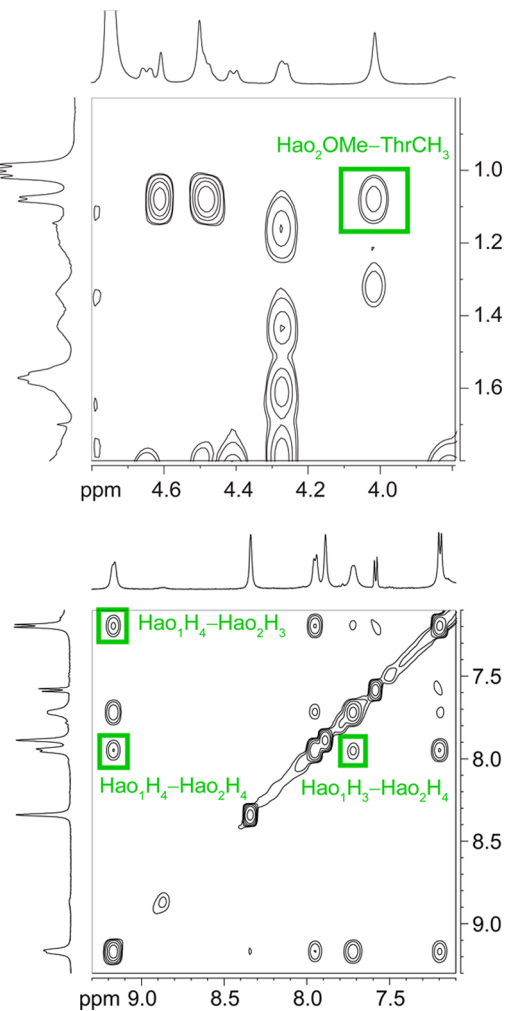


Figure 6. Selected expansions of the NOESY spectrum of macrocyclic β -sheet peptide **2a** at 8.0 mM in D_2O at 500 MHz and 300.5 K. Key interlayer NOEs associated with tetramerization are highlighted in green.

Addition of salt ($NaCl$) augments tetramer formation, suggesting that intermolecular ionic repulsion is partially responsible for the diminished tetramerization of macrocyclic β -sheet **3**. Without $NaCl$, macrocyclic β -sheet **3** is 46% tetramerized at 4.0 mM; with 25 mM $NaCl$, it is 70% tetramerized; with 150 mM $NaCl$, it is 80% tetramerized (Figure S6 and Table S3 in the SI).⁴³ The loss of hydrophobic interactions between the methyl group of threonine and the methoxy group of Hao_2 may also contribute to the diminished stability of the tetramer of macrocyclic β -sheet **3**.

Diffusion-ordered spectroscopy (DOSY) NMR studies support the formation of a tetrameric species.^{44,45} Measurement of the DOSY spectrum of macrocyclic β -sheet peptide **2a** in D_2O at 2.0 mM and 8.0 mM and 298 K gave a diffusion coefficient of $10.0 \times 10^{-7} \text{ cm}^2/\text{s}$ and $10.1 \times 10^{-7} \text{ cm}^2/\text{s}$, respectively, for the oligomer.^{46,47} The diffusion coefficient does not vary from 2.0 mM to 8.0 mM, suggesting the presence of a single oligomerization state. The low concentration of monomer precluded measurement of its diffusion coefficient for comparison. Measurement of the DOSY spectrum of macrocyclic β -sheet peptide **3** in D_2O at 2.0 mM and 298 K gave a diffusion coefficient of $16.4 \times 10^{-7} \text{ cm}^2/\text{s}$ for the corresponding monomer. Consistent with tetramer formation, the diffusion

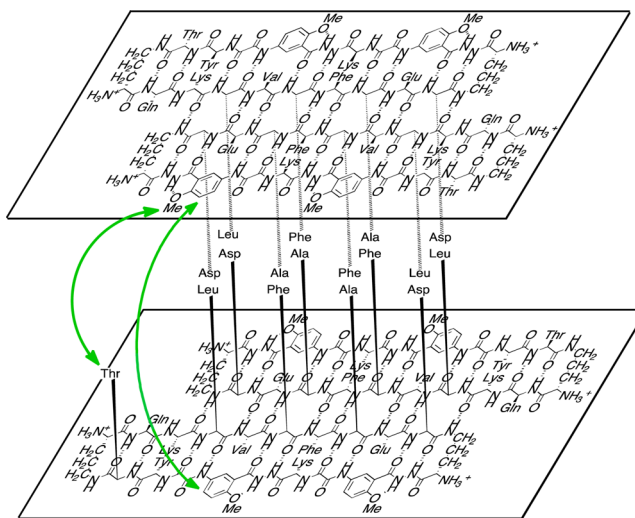


Figure 7. Illustration of the tetramer formed as a sandwich-like assembly of two hydrogen-bonded dimers of macrocyclic β -sheet peptide **2a** in aqueous solution. The green arrow shows key NOEs between the layered β -sheets. Four sets of these interactions can occur in the tetramer. (For clarity, only one set is shown.) Macrocylic β -sheet peptide **1** forms a similar sandwich-like tetramer in solution.

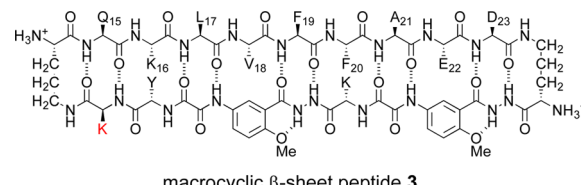
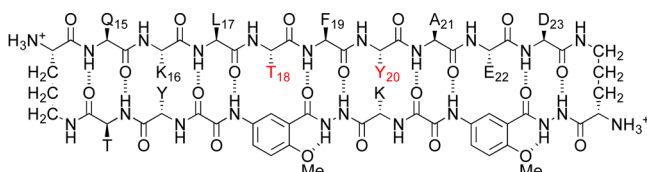
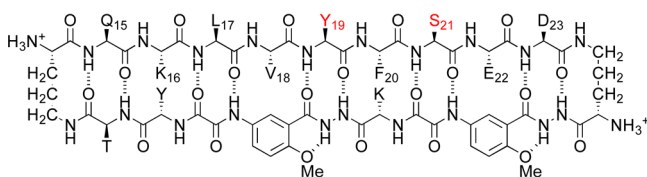


Figure 8. Expansions of the 1H NMR spectra of macrocyclic β -sheet peptide **3** at various concentrations in D_2O at 500 MHz and 298 K. Noteworthy characteristic resonances of the monomer and the oligomer are labeled and highlighted with dashed lines.

coefficient of the oligomer of macrocyclic β -sheet peptide **2a** is 0.61 times that of the monomer of macrocyclic β -sheet peptide **3**.^{45,47–49}

3. Facial Control of Tetramerization in Macrocylic β -Sheet Peptides **2b and **2c**.** To further study the assembly of the tetramer, we mutated residues on the LFA and VF faces to

examine how the hydrophobic residues on each face control tetramer formation. We created two double mutants of **2a**, in which either the hydrophobic residues V₁₈ and F₂₀ or the hydrophobic residues F₁₉ and A₂₁ were rendered more hydrophilic by hydroxylation. In double mutant **2b**, V₁₈ was replaced with threonine and F₂₀ was replaced with tyrosine (V₁₈T,F₂₀Y). In double mutant **2c**, F₁₉ was replaced with tyrosine and A₂₁ was replaced with serine (F₁₉Y,A₂₁S).

macrocyclic β -sheet peptide **2b**macrocyclic β -sheet peptide **2c**

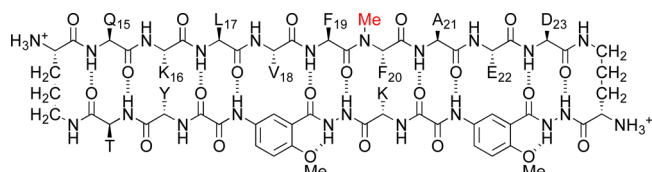
The ¹H NMR spectrum of the V₁₈T,F₂₀Y double mutant **2b** is strikingly similar to that of macrocyclic β -sheet **2a** (Figure 2), indicating that **2a** and **2b** fold and oligomerize in a similar fashion in aqueous solution. The methyl resonances from L₁₇ and A₂₁ appear unusually upfield, the aromatic resonances from F₁₉ also appear unusually upfield, and many of the amino acid α -protons appear unusually downfield. The ¹H NMR spectra of both compounds reflect similar monomer–oligomer equilibria. At 0.1 mM, the monomer predominates and only small resonances from the tetramer are present; at 1.0 mM, the resonances from the tetramer predominate and only small resonances from the monomer are present. Thus, V₁₈T,F₂₀Y double mutation does not substantially alter the equilibrium constant for tetramer formation.

The ¹H NMR spectrum of the F₁₉Y,A₂₁S double mutant **2c** differs markedly from those of **2a** and **2b** (Figure S7 in the SI). The methyl resonances from L₁₇ do not appear unusually upfield and the amino acid α -protons do not appear unusually downfield. These observations indicate that F₁₉Y,A₂₁S double mutation disrupts the formation of the tetramer. The ¹H NMR spectrum of macrocyclic β -sheet **2c** shows some minor broadened resonances at 2.0 mM, which diminish at lower concentrations, suggesting that some weaker nonspecific self-association may persist when tetramer formation is disrupted.

The dramatic differences between macrocyclic β -sheets **2b** and **2c** further demonstrate the importance of hydrophobic interactions of the LFA face of the macrocycle in tetramer formation. When the LFA face is hydroxylated, tetramer formation is disrupted, but when the VF face is hydroxylated, tetramer formation is not affected.

4. Hydrogen-Bonding Edge Control of Tetramerization in Macrocytic β -Sheet Peptide 4. To probe the role of hydrogen bonding in tetramer formation, we blocked the hydrogen-bonding edge of the macrocycle by *N*-methylation. Macrocytic β -sheet **4** is a homologue of macrocyclic β -sheet **2a** with *N*-methylphenylalanine in place of phenylalanine at position 20. The F₂₀F^{N-Me} mutation is designed to block formation of the hydrogen-bonded dimer and thus the

assembly of a tetramer comprising a dimer of hydrogen-bonded dimers. The ¹H NMR spectrum of macrocyclic β -sheet **4** also differs markedly from those of **2a** and **2b** (Figure S7 in the SI). The methyl resonances from L₁₇ and A₂₁ do not appear unusually upfield and the amino acid α -protons do not appear unusually downfield. The disruption of tetramer formation by *N*-methylation demonstrates that hydrogen bonding is also essential for tetramer formation.

macrocyclic β -sheet peptide **4**

5. Diffusion Studies of Macrocytic β -Sheet Peptides

1–4. DOSY NMR studies of macrocyclic β -sheets **1–4** suggest that **1**, **2a**, and **2b** are tetrameric at millimolar concentrations, while **2c**, **3**, and **4** are monomeric.^{44,45,47} As mentioned above, the oligomeric **2a** exhibits a diffusion coefficient of 10.0×10^{-7} cm²/s in D₂O at 298 K, while monomeric **3** exhibits a diffusion coefficient of 16.4×10^{-7} cm²/s. The ratio of these diffusion coefficients — about 0.6 — is consistent with tetramer formation.^{45,47–49} Macrocytic β -sheets **1** and **2b** exhibit diffusion coefficients similar to that of **2a**, while macrocyclic β -sheets **2c** and **4** exhibit diffusion coefficients similar to that of **3** (Table 1).

Table 1. Diffusion Coefficients (D) of Peptides 1–4 in D₂O at 298 K

peptide	MW _{monomer} ^a (Da)	MW _{tetramer} ^a (Da)	D (10^{-7} cm ² /s)	oligomer state
1	2232	8929	10.1^b	tetramer
2a	2169	8677	10.0^b	tetramer
			10.1^c	
2b	2187	8749	10.3^b	tetramer
			10.1^c	
2c	2201	NA	16.5^b	monomer
3	2196	8785	16.4^b	monomer
4	2183	NA	17.6^b	monomer

^aMolecular weight calculated for the neutral (uncharged) macrocycle.

^bDiffusion coefficient measured at 2.0 mM. ^cDiffusion coefficient measured at 8.0 mM.

6. Analytical Ultracentrifugation Studies of Macrocytic β -Sheet Peptide 2b. To corroborate the DOSY studies, we performed analytical ultracentrifugation (AUC) sedimentation velocity studies on macrocyclic β -sheet **2b**.^{50–53} The AUC studies are best performed in nonzero ionic strength to avoid nonideality resulting from charge interactions between the large cationic molecules. Thus, we performed AUC sedimentation velocity studies in the presence of salt, using 0.10, 0.30, and 0.66 mM solutions of macrocycle **2b** in H₂O containing 25 mM NaCl at 293 K. The sedimentation velocity data fit well to a reversible monomer–tetramer equilibrium with slow exchange on the time scale of the experiment (hours). The tetramer predominated at all three concentrations, with the greatest fraction of monomer present at 0.10 mM. Analysis of the data from the 0.10 mM experiment gave a good fit to a monomer–tetramer equilibrium with a 2.14 kDa

monomer and a 8.55 kDa tetramer and a K_{assoc} of 1.93×10^{14} M⁻³.^{54,55} (For details see the SI.)

7. Folding of Macroyclic β -Sheet Peptides 1–4. The magnetic anisotropy of the diastereotopic δ -protons of the δ -linked ornithine turn units in the ¹H NMR spectra reflect that the tetramers of 1a, 2a, and 2b form well-folded β -sheets, while the monomers of 2c, 3, and 4 are only partially folded. In a well-folded macrocyclic β -sheet, the difference in the chemical shifts ($\Delta\delta$) of the diastereotopic *pro-S* and *pro-R* δ -protons of the δ -linked ornithine turn units (^δOrn) is about 0.6 ppm in aqueous solution.^{38,47,56} Values substantially lower than 0.6 ppm reflect the formation of partially folded macrocyclic β -sheet structures. At 2.0 mM and 298 K in D₂O, the tetramers of 1, 2a, and 2b exhibit large magnetic anisotropies, while the monomers of 2c, 3, and 4 exhibit smaller magnetic anisotropies (Table 2). Thus, oligomerization promotes folding.

Table 2. Magnetic Anisotropies of the δ -Protons of the δ -Linked Ornithine Turn Units of Peptides 1–4 in D₂O at 298 K

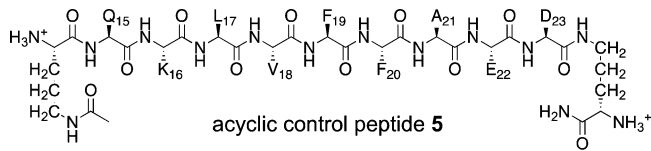
peptide	^δ Orn ₁ $\Delta\delta$ (ppm)	^δ Orn ₂ $\Delta\delta$ (ppm)	folding
1 ^a	0.64	0.70	folded tetramer
2a ^a	0.64	0.72	folded tetramer
2b ^a	0.64	0.70	folded tetramer
2c ^a	0.23 ^d	0.45 ^d	partially folded monomer
3 ^b	0.54 ^d	0.24 ^d	partially folded monomer
3 ^c	0.58 ^d	0.66 ^d	folded tetramer
4 ^a	0.30 ^d	0.32 ^d	partially folded monomer

^aOligomer at 2.0 mM. ^bMonomer at 2.0 mM. ^cOligomer at 8.0 mM.

^dAssignment of ^δOrn₁ and ^δOrn₂ is arbitrary.

To further investigate the folding and oligomerization of macrocyclic β -sheet 2a, we compared the ¹H NMR chemical shifts of the α -protons of the 2a tetramer to those of acyclic control peptide 5.⁵⁷ Peptide 5 contains the A β _{15–23} nonapeptide and two δ -linked ornithine turn units but lacks the lower template strand. The α -proton resonances of A β _{15–23} in the 2a tetramer appear 0.04–1.04 ppm downfield of those of acyclic control, with an average downfield shifting of 0.66 ppm (Figures 9 and S8 in the SI). The large downfield shifting of the

α -protons suggests the formation of a well-folded β -sheet structure.



In contrast, the α -proton resonances of the monomer of 2a are not nearly as far downfield shifted. Although it is not feasible to identify all of the α -proton resonances of the monomer of 2a because the tetramer predominates even at submillimolar concentrations, it is possible to do so in the close homologue 3, which is largely monomeric at low millimolar concentrations. The α -proton resonances of A β _{15–23} in the 3 monomer show far less downfield shifting, with an average of only 0.13 ppm (Figures 9 and S8 in the SI). The smaller downfield shifting of the α -protons of the monomers of 2a and 3 reflects the formation of β -sheet structures that are only partially folded.

DISCUSSION

The tetramers formed by macrocyclic β -sheets containing the A β _{15–23} nonapeptide are remarkable. Although the individual peptide monomer units are only partially folded, the tetramers that form exhibit secondary, tertiary, and quaternary structure reminiscent of proteins. The unusually well-defined structures of the tetramers are reflected in the strong NOEs observed and in the large magnetic anisotropies of the L₁₇, F₁₉, and A₂₁ side chains and many of the α -protons in the ¹H NMR spectra.

To gain further insight into the structure of the tetramers formed by the macrocyclic β -sheets in aqueous solution, we used the X-ray crystallographic structure of the tetramer of macrocyclic β -sheet 1 to create a model of the solution-state tetramer of macrocyclic β -sheet 2a. We generated the initial coordinates for the model in PyMOL by (1) changing the *p*-bromophenylalanine of 1 to tyrosine, (2) shifting the crystallographic dimers out of alignment by two residues toward the C-termini, (3) moving the dimers to pack through the LFA faces instead of the VF faces, (4) selecting appropriate rotamers of F₂₀, and (5) orienting the dimers to approximately match the observed interlayer NOEs between the methoxy group of Hao₂ and the methyl group of threonine. We then generated a minimum-energy structure (local minimum) of the tetramer in MacroModel with the Maestro user interface using the MMFFs force field with GB/SA water solvation, minimizing first with distance constraints to match the observed NOEs between α -protons (Figure 3) and between the layers of the β -sheets (Figures 6 and 7) and then without constraints.

Figure 10 illustrates the resulting model of the tetramer. The tetramer consists of a dimer of hydrogen-bonded dimers and is essentially symmetrical, consisting of four roughly symmetrical monomers arranged in roughly *D*₂ symmetry. Residues L₁₇, F₁₉, and A₂₁ of the dimers pack tightly to form a hydrophobic core within the tetramer (Figure 10B and C). The methyl group of A₂₁ sits over the phenyl group of F₁₉ in the opposing layer of the sandwich-like structure, consistent with the observed upfield shifting of the methyl resonance of A₂₁ in the ¹H NMR spectrum. The *pro-S* methyl group of L₁₇ sits over the aromatic ring of Hao₂ in the opposing layer, consistent with the pronounced upfield shifting of one of the methyl resonances of L₁₇ in the ¹H NMR spectrum. The methyl group of the threonine is close to the methoxy group of Hao₂, and Hao₁ is

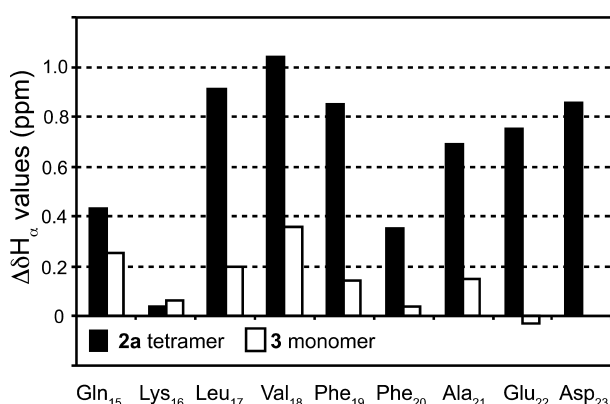


Figure 9. Downfield shifting of the ¹H NMR α -proton resonances of the 2a tetramer and the 3 monomer, relative to acyclic control 5. The ¹H NMR spectrum of 2a was recorded at 8.0 mM in D₂O at 500 MHz and 300.5 K. The ¹H NMR spectra of 3 and 5 were recorded at 2.0 and 1.2 mM, respectively, in D₂O at 500 MHz and 298 K.

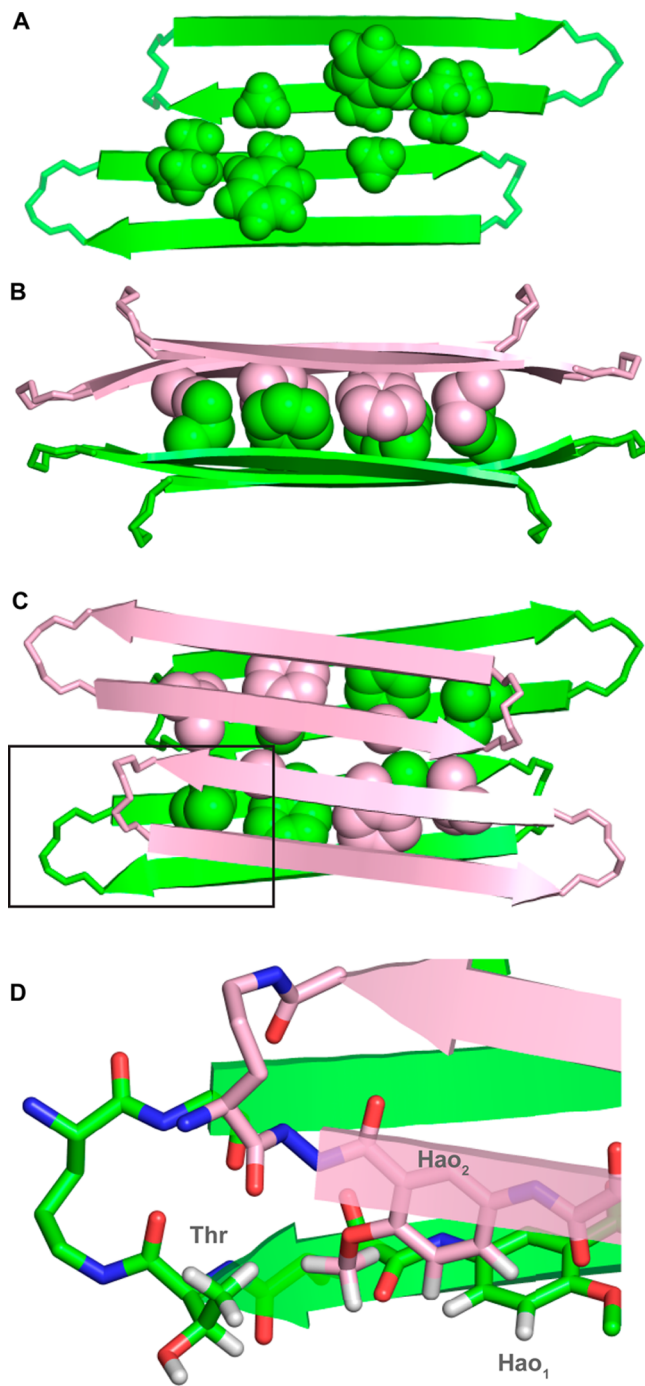


Figure 10. Model of macrocyclic β -sheet peptide **2a** as a tetramer, based on the NOE cross peaks of **2a** and the X-ray crystallographic structure of **1**. (A) Hydrogen-bonded dimers within the tetramer. The hydrogen-bonded dimers are antiparallel and shifted out of alignment by two residues toward the C-termini. Residues L₁₇, F₁₉, and A₂₁ of the hydrophobic core are shown (the LFA face). (B) Side view of **2a** as a tetramer. (C) Top view of **2a** as a tetramer. The LFA faces that form the hydrophobic core of the tetramer are shown. (D) Detail of the contacts between threonine, Hao₁, and Hao₂, which give rise to the interlayer NOE crosspeaks that are shown in Figure 6.

close to Hao₂, consistent with the observed NOEs between these groups (Figure 10D and Figure 6).

The solution-state tetramers formed by macrocyclic β -sheets **1**, **2a**, and **2b** differ from the solid-state tetramer observed for macrocyclic β -sheet **1** in three notable ways: Although both

tetramers comprise antiparallel β -sheet dimers, the solution-state dimers are out of register, shifted out of alignment by two residues toward the C-termini, while the solid-state dimers are in register, with all residues aligned (Figure 11). The solution-

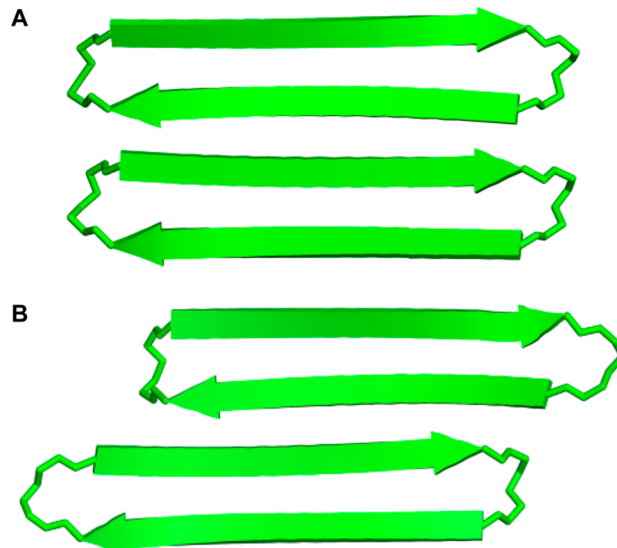


Figure 11. Model of macrocyclic β -sheet peptide **2a** and the X-ray crystallographic structure of **1** as dimers. (A) X-ray crystallographic structure of hydrogen-bonded dimers of **1** that are antiparallel and fully aligned. (B) Solution-state structure of hydrogen-bonded dimers of **2a** that are antiparallel and shifted out of alignment by two residues toward the C-termini.

state dimers are sandwiched through the LFA faces, while the solid-state dimers are sandwiched through the VF faces (Figure 12). The two solution-state dimers that form the tetramer are nearly parallel to each other, while the two solid-state dimers are nearly orthogonal; the former are oriented at roughly 15°, while the latter are oriented at roughly 83° (Figure 12).

The differences between the solution-state tetramer and the solid-state tetramer may reflect the need to maximize hydrophobic contacts in aqueous solution. In aqueous solution, hydrophobic contacts within the tetramer are important. The LFA face of the dimer presents six hydrophobic residues from $A\beta_{15-23}$, while the VF face presents only four (Figure 12).⁵⁸ Hydrophobic contact is maximized in the aqueous tetramer through contact between these six residues. The bulky hydrophobic side chains of L₁₇ and F₁₉ pack well with the small hydrophobic side chain of A₂₁ in the opposing dimer of the tetramer. In the solid state, the tetramer is part of a lattice in which there are additional intermolecular contacts. The tetramers are in contact with other tetramers, as well as with water and organic cocrystallants, and these contacts likely help stabilize the tetramer. Differences in pH and protonation state may also be important in the differences between the solution-state and solid-state tetramers.

The differing morphology of the solution-state and solid-state tetramers is significant, because it may provide a glimpse into some of the structural bases for polymorphism among $A\beta$ oligomers in Alzheimer's disease. Polymorphism has previously been observed at atomic resolution in $A\beta$ fibrils, but not in oligomers.⁵⁹⁻⁶² Because little is known about the structures of amyloid oligomers, little is known about the structural bases of oligomer polymorphism. Much of what is currently known about amyloid oligomer polymorphism focuses on differences

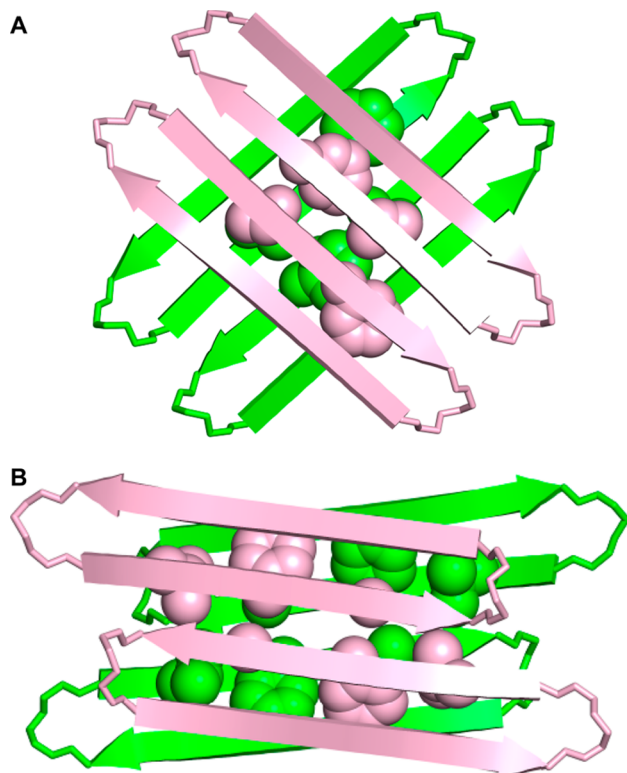


Figure 12. Model of macrocyclic β -sheet peptide **2a** and the X-ray crystallographic structure of **1** as tetramers. (A) Top view of the X-ray crystallographic structure of **1** as a tetramer. Residues V₁₈ and F₂₀ of the hydrophobic core are shown (the VF face). One rotamer of residue F₂₀ for each monomer is shown. (B) Top view of solution-state structure of **2a** as a tetramer. Residues L₁₇, F₁₉, and A₂₁ of the hydrophobic core are shown (the LFA face).

in reactivity toward oligomer-specific antibodies or differences in size and shape that can be observed by electron microscopy, atomic-force microscopy, gel electrophoresis, or mass spectrometry. These techniques do not provide detail at atomic resolution. The contrasting structures of the solution-state and solid-state tetramers described here demonstrate subtle differences among oligomers that can be observed at atomic resolution. Differing facial pairings of the β -sheets give rise to unique stable structures. Differing alignment of the β -strands within the β -sheets also gives rise to unique structures. While not seen in the two types of tetramers here, both parallel and antiparallel β -sheet structures may also be possible.

CONCLUSION

Macrocyclic β -sheet peptides containing the A β _{15–23} nonapeptide exhibit rich supramolecular chemistry, forming tetramers with well-defined structures in aqueous solution and in the solid state.⁶³ The solution-state and solid-state tetramers exhibit noteworthy polymorphism, differing in the alignment of the monomers within the hydrogen-bonded dimers, the faces of the hydrogen-bonded dimers involved in tetramer formation, and the rotational orientation of the hydrogen-bonded dimers within the tetramers (Figure 13). Both hydrogen bonding and hydrophobic interactions are important in tetramer formation. Residues L₁₇, F₁₉, and A₂₁ are critical in the formation of the hydrophobic core of the tetramers in solution, and the size complementarity of the small

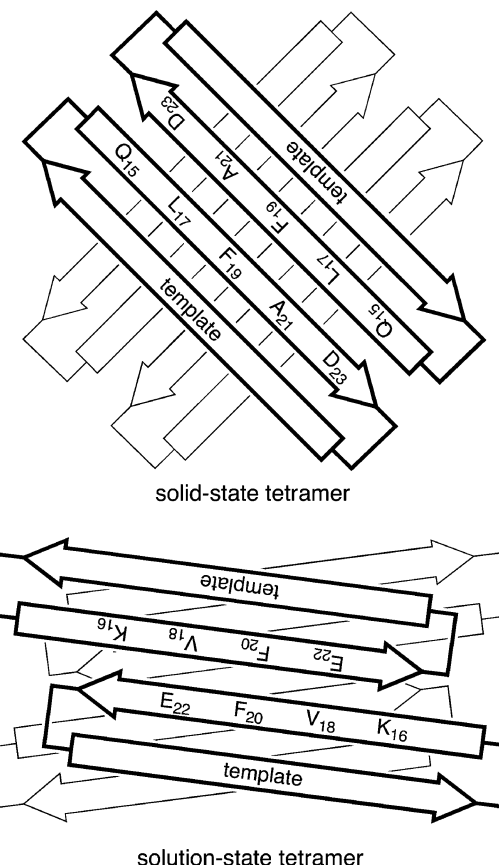


Figure 13. Cartoon illustrating the structure of the solid-state tetramer of macrocyclic β -sheet **1** (top), and the solution-state tetramer of macrocyclic β -sheets **1** and **2a** (bottom). The VF faces form the inner hydrophobic core of the solid-state tetramer of **1**, and the LFA faces form the outer surface. The LFA faces form the inner hydrophobic core of the solution-state tetramer of **1** and **2a**, and the VF faces form the outer surface.

A₂₁ residue and large L₁₇ and F₁₉ residues may play a special role in their stability.

The supramolecular assembly of amyloidogenic peptides to form soluble oligomers is almost impossible to study at atomic resolution with natural full-length amyloidogenic peptides, because the oligomers that form are heterogeneous in size and morphology and because the oligomers are dynamic and can ultimately form insoluble amyloid. Chemical model systems that limit uncontrolled supramolecular assembly and contain important segments of the amyloidogenic peptides can help identify modes in which the peptides interact. We anticipate that chemical model systems based on macrocyclic peptides will prove widely useful in elucidating the supramolecular assembly and oligomer formation of other amyloidogenic peptides. We look forward to reporting these findings in due course.

ASSOCIATED CONTENT

S Supporting Information

Experimental procedures, NMR spectra, mass spectra, and HPLC traces for peptides **2–5** and hitherto unreported data for peptide **1**. This material is available free of charge via the Internet at <http://pubs.acs.org>.

AUTHOR INFORMATION

Corresponding Author

jsnowick@uci.edu

Notes

The authors declare no competing financial interest.

ACKNOWLEDGMENTS

We thank Dr. Phil Dennison and Prof. Melanie Cocco for assistance in running 800 MHz NMR experiments and Mr. Virgil Schirf for assistance in running AUC experiments. J.S.N and J.D.P. thank the National Institutes of Health for grant support (5R01GM097562). J.D.P. thanks UCI for fellowship support. B.D. thanks the National Science Foundation (Grants ACI-1339649, OCI-1032742, and MCB-070039) for supporting the UltraScan software development.

REFERENCES

- (1) Kayed, R.; Head, E.; Thompson, J. L.; McIntire, T. M.; Milton, S. C.; Cotman, C. W.; Glabe, C. G. *Science* **2003**, *300*, 486–489.
- (2) Lacor, P. N.; Buniel, M. C.; Chang, L.; Fernandez, S. J.; Gong, Y.; Viola, K. L.; Lambert, M. P.; Velasco, P. T.; Bigio, E. H.; Finch, C. E.; Krafft, G. A.; Klein, W. L. *J. Neurosci.* **2004**, *24*, 10191–11200.
- (3) Haass, C.; Selkoe, D. J. *Nat. Rev. Mol. Cell Biol.* **2007**, *8*, 101–112.
- (4) Walsh, D. M.; Selkoe, D. J. *J. Neurochem.* **2007**, *101*, 1172–1184.
- (5) Glabe, C. G. *J. Biol. Chem.* **2008**, *283*, 29639–29643.
- (6) Kayed, R.; Canto, I.; Breydo, L.; Rasool, S.; Lukacsovich, T.; Wu, J.; Albay, R., III; Pensalfini, P.; Yeung, S.; Head, E.; Marsh, J. L.; Glabe, C. *Mol. Neurodegener.* **2010**, *5*, 1–10.
- (7) Umeda, T.; Tomiyama, T.; Sakama, N.; Tanaka, S.; Lambert, M. P.; Klein, W. L.; Mori, H. *J. Neurosci. Res.* **2011**, *89*, 1031–1042.
- (8) Fändrich, M. *J. Mol. Biol.* **2012**, *421*, 427–440.
- (9) Benilova, I.; Karran, E.; De Strooper, B. *Nat. Neurosci.* **2012**, *15*, 349–357.
- (10) Nussbaum, J. M.; Schilling, S.; Cynis, H.; Silva, A.; Swanson, E.; Wangsanut, T.; Tayler, K.; Wiltgen, B.; Hatami, A.; Rönicke, R.; Reymann, K.; Hutter-Paier, B.; Alexandru, A.; Jagla, W.; Graubner, S.; Glabe, C. G.; Demuth, H.-U.; Bloom, G. S. *Nature* **2012**, *485*, 651–655.
- (11) Chromy, B. A.; Nowak, R. J.; Lambert, M. P.; Viola, K. L.; Chang, L.; Velasco, P. T.; Jones, B. W.; Fernandez, S. J.; Lacor, P. N.; Horowitz, P.; Finch, C. E.; Krafft, G. A.; Klein, W. L. *Biochemistry* **2003**, *42*, 12749–12760.
- (12) Cleary, J. P.; Walsh, D. M.; Hofmeister, J. J.; Shankar, G. M.; Kuskowski, M. A.; Selkoe, D. J.; Ashe, K. H. *Nat. Neurosci.* **2005**, *8*, 79–84.
- (13) Lesné, S.; Koh, M. T.; Kotilinek, L.; Kayed, R.; Glabe, C. G.; Yang, A.; Gallagher, M.; Ashe, K. H. *Nature* **2006**, *440*, 352–357.
- (14) Shankar, G. M.; Li, S.; Mehta, T. H.; Garcia-Munoz, A.; Shepardson, N. E.; Smith, I.; Brett, F. M.; Farrell, M. A.; Rowan, M. J.; Lemer, C. A.; Regan, C. M.; Walsh, D. M.; Sabatini, B. L.; Selkoe, D. J. *Nat. Med.* **2008**, *14*, 837–842.
- (15) Ono, K.; Condron, M. M.; Teplow, D. B. *Proc. Natl. Acad. Sci. U.S.A.* **2009**, *106*, 14745–14750.
- (16) Selkoe, D. J. *Behav. Brain Res.* **2008**, *192*, 106–113.
- (17) Larson, M. E.; Lesné, S. E. *J. Neurochem.* **2012**, *192* (Suppl. 1), 125–139.
- (18) Vivekanandan, S.; Brender, J. R.; Lee, S. Y.; Ramamoorthy, A. *Biochem. Biophys. Res. Commun.* **2011**, *411*, 312–316.
- (19) Bernstein, S. L.; Dupuis, N. F.; Lazo, N. D.; Wyttenbach, T.; Condron, M. M.; Bitan, G.; Teplow, D. B.; Shea, J.-E.; Ruotolo, B. T.; Robinson, C. V.; Bowers, M. T. *Nat. Chem.* **2009**, *1*, 326–331.
- (20) Miller, Y.; Ma, B.; Nussinov, R. *Chem. Rev.* **2010**, *110*, 4820–4838.
- (21) Lührs, T.; Ritter, C.; Adrian, M.; Riek-Lohr, D.; Bohrmann, B.; Döbeli, H.; Schubert, D.; Riek, R. *Proc. Natl. Acad. Sci. U.S.A.* **2005**, *102*, 17342–17347.
- (22) Petkova, A. T.; Yau, W.-M.; Tycko, R. *Biochemistry* **2006**, *45*, 498–512.
- (23) Cerf, E.; Sarroukh, R.; Tamamizu-Kato, S.; Breydo, L.; Derclaye, S.; Dufrênes, Y. V.; Narayanaswami, V.; Goormaghtigh, E.; Ruysschaert, J.-M.; Raussens, V. *Biochem. J.* **2009**, *421*, 415–423.
- (24) Chimon, S.; Shaibat, M. A.; Jones, C. R.; Calero, D. C.; Aizezi, B.; Ishii, Y. *Nat. Struct. Mol. Biol.* **2010**, *14*, 1157–1164.
- (25) Strodel, B.; Lee, J. W.; Whittleston, C. S.; Wales, D. J. *J. Am. Chem. Soc.* **2010**, *132*, 13300–13312.
- (26) Streletsov, V. A.; Varghese, J. N.; Masters, C. L.; Nuttall, S. D. *J. Neurosci.* **2011**, *31*, 1419–1426.
- (27) Laganowsky, A.; Liu, C.; Sawaya, M. R.; Whitelegge, J. P.; Park, J.; Zhao, M.; Pensalfini, A.; Soriaga, A. B.; Landau, M.; Keng, P. K.; Cascio, D.; Glabe, C. G.; Eisenberg, D. *Science* **2012**, *335*, 1228–1231.
- (28) Apostol, M. I.; Perry, K.; Surewicz, W. K. *J. Am. Chem. Soc.* **2013**, *135*, 10202–10205.
- (29) Hoyer, W.; Grönwall, C.; Jonsson, A.; Ståhl, S.; Härd, T. *Proc. Natl. Acad. Sci. U.S.A.* **2008**, *105*, 5099–5104.
- (30) Sandberg, A.; Luheshi, L. M.; Sölvander, S.; de Barros, T. P.; Macao, B.; Knowles, T. P. J.; Biverstål, H.; Lendel, C.; Ekholm-Pettersson, F.; Dubnovitsky, A.; Lannfelt, L.; Dobson, C. M.; Härd, T. *Proc. Natl. Acad. Sci. U.S.A.* **2010**, *107*, 15595–15600.
- (31) Yu, L.; Edalji, R.; Harlan, J. E.; Holzman, T. F.; Lopez, A. P.; Labkovsky, B.; Hillen, H.; Barghorn, S.; Ebert, U.; Richardson, P. L.; Miesbauer, L.; Solomon, L.; Bartley, D.; Walter, K.; Johnson, R. W.; Hajduk, P. J.; Olejniczak, E. T. *Biochemistry* **2009**, *48*, 1870–1877.
- (32) Horn, A. H. C.; Sticht, H. *J. Phys. Chem. B* **2010**, *114*, 2219–2226.
- (33) Xu, J.; Zhang, J. Z. H.; Xiang, Y. *J. Phys. Chem. A* **2013**, *117*, 6373–6379.
- (34) Miller, Y.; Ma, B.; Tsai, C.-J.; Nussinov, R. *Proc. Natl. Acad. Sci. U.S.A.* **2010**, *107*, 14128–14133.
- (35) We began these studies through a fruitful collaboration with the laboratory of Professor David Eisenberg: (a) Zheng, J.; Liu, C.; Sawaya, M. R.; Vadla, B.; Khan, S.; Woods, R. J.; Eisenberg, D.; Goux, W. J.; Nowick, J. S. *J. Am. Chem. Soc.* **2011**, *133*, 3144–3157. (b) Liu, C.; Sawaya, M. R.; Cheng, P.-N.; Zheng, J.; Nowick, J. S.; Eisenberg, D. *J. Am. Chem. Soc.* **2011**, *133*, 6736–6744. (c) Cheng, P.-N.; Liu, C.; Zhao, M.; Eisenberg, D.; Nowick, J. S. *Nat. Chem.* **2012**, *4*, 927–933. (d) Liu, C.; Zhao, M.; Jiang, L.; Cheng, P.-N.; Park, J.; Sawaya, M. R.; Pensalfini, A.; Gou, D.; Berk, A. J.; Glabe, C. G.; Nowick, J. S.; Eisenberg, D. *Proc. Natl. Acad. Sci. U.S.A.* **2012**, *109*, 20913–20918.
- (36) (a) Zheng, J.; Baghkhalian, A. M.; Nowick, J. S. *J. Am. Chem. Soc.* **2013**, *135*, 6846–6852. (b) Buchanan, L. E.; Dunkelberger, E. B.; Tran, H. Q.; Cheng, P.-N.; Chiu, C.-C.; Cao, P.; Raleigh, D. P.; de Pablo, J. J.; Nowick, J. S.; Zanni, M. T. *Proc. Natl. Acad. Sci. U.S.A.* **2013**, *110*, 19285–19290.
- (37) Pham, J. D.; Chim, N.; Goulding, C. W.; Nowick, J. S. *J. Am. Chem. Soc.* **2013**, *135*, 12460–12467.
- (38) Nowick, J. S.; Brower, J. O. *J. Am. Chem. Soc.* **2003**, *125*, 876–877.
- (39) Nowick, J. S.; Chung, D. M.; Maitra, K.; Maitra, S.; Stigers, K. D.; Sun, Y. *J. Am. Chem. Soc.* **2000**, *122*, 7654–7661.
- (40) An EXSY experiment (2.0 mM in D₂O at 350 K with a mixing time of 200 ms) shows that the oligomer is in equilibrium with the monomer. Notably, crosspeaks from chemical exchange between the L₁₇CH₃, V₁₈CH₃, and A₂₁CH₃ resonances of the monomer and the oligomer are seen in the EXSY spectrum. Additional EXSY crosspeaks involving the aromatic resonances from F₁₉ and various α -proton resonances are also seen. (SI)
- (41) At 0.2 mM, the molar concentration of the tetramer is roughly one-fourth the molar concentration of the monomer (i.e., $[2a_4] \approx 0.025$ mM and $[2a] \approx 0.1$ mM). These concentrations correspond to an equilibrium constant K_{assoc} for monomer-to-tetramer association of roughly $2.5 \times 10^{11} \text{ M}^{-3}$.
- (42) Additional interlayer NOEs consistent with the sandwich-like assembly shown in Figure 7 are summarized in Table S1 in the SI.
- (43) Addition of salt also augments tetramer formation of macrocyclic β -sheet 2a: Without NaCl, macrocyclic β -sheet 2a is 56%

tetramerized at 0.3 mM; with 25 mM NaCl, it is 82% tetramerized (Figure S5 and Table S2 in the SI).

(44) (a) Berger, S.; Braun, S. *200 and More NMR Experiments: A Practical Course*; Wiley-VCH: Weinheim, 2004; pp 515–517. (b) Findeisen, M.; Berger, S. *50 and More Essential NMR Experiments*; Wiley-VCH: Weinheim, 2012; pp 163–166.

(45) (a) Altieri, A. S.; Hinton, D. P.; Byrd, R. A. *J. Am. Chem. Soc.* **1995**, *117*, 7566–7567. (b) Johnson, C. S. *Progr. NMR Spectrosc.* **1999**, *34*, 203–256. (c) Yao, S.; Howlett, G. J.; Norton, R. S. *J. Biomol. NMR* **2000**, *16*, 109–119. (d) Cohen, Y.; Avram, L.; Frish, L. *Angew. Chem., Int. Ed.* **2005**, *44*, 520–554. (e) Cohen, Y.; Avram, L.; Evan-Salem, T.; Slovak, S.; Shemesh, N.; Frish, L. In *Analytical Methods in Supramolecular Chemistry*, 2nd ed.; Schalley, C. A., Ed.; Wiley-VCH: Weinheim, 2012; pp 197–285.

(46) As is expected, the diffusion coefficient of the tetramer of **2a** is slightly lower than that of a lighter tetramer of a smaller peptide that we had studied previously (12.0×10^{-7} cm²/s for a 6.4 kDa tetramer vs 10.0×10^{-7} cm²/s for the 8.9 kDa tetramer of **2a**).

(47) Khakshoor, O.; Demeler, B.; Nowick, J. S. *J. Am. Chem. Soc.* **2007**, *129*, 5558–5569.

(48) Teller, D. C.; Swanson, E.; DeHaen, C. *Methods Enzymol.* **1979**, *61*, 103–124.

(49) Polson, A. *J. Phys. Colloid Chem.* **1950**, *54*, 649–652.

(50) Analytical ultracentrifugation sedimentation velocity experiments characterize the solution-state behavior of macromolecules and can identify dynamic processes such as mass-action driven reversible associations by observing the sedimentation and diffusion behavior of all species in a mixture and report their partial concentrations, molecular weights, and anisotropies. Analysis of multiple loading concentrations can reveal shifts in the sedimentation profile, corresponding to increasing amounts of higher oligomeric forms in response to mass action. Reversible reactions can be fitted directly to solutions of the Lamm equation to obtain the equilibrium coefficients of the reactions, and to obtain mass and anisotropy of the reacting species.

(51) Demeler, B. *Current Protocols in Protein Science*; Wiley: Hoboken, NJ, 2010; unit 7.13, Chapter 7.

(52) Demeler, B.; Brookes, E.; Wang, R.; Schirf, V.; Kim, C. A. *Macromol. Biosci.* **2010**, *7*, 775–782.

(53) Cao, W.; Demeler, B. *Biophys. J.* **2008**, *95*, 54–65.

(54) A K_{assoc} of 1.93×10^{14} M⁻³ corresponds to a 1:1 molar ratio of monomer and tetramer at 0.086 mM total concentration of **2b** and a 4:1 molar ratio of monomer and tetramer at 0.022 mM total concentration of **2b**. The stronger self-association of **2b** under these conditions, as compared to the NMR studies shown in Figure 5, may be explained by the NaCl and lower temperature used for the AUC studies.

(55) Macrocyclic β -sheet **2a** was found to form high-molecular weight aggregates when subjected to AUC studies under similar conditions. The formation of high-molecular weight aggregates may reflect enhanced self-association and aggregation promoted by salt (NaCl).

(56) Woods, J. R.; Brower, J. O.; Castellanos, E.; Hashemzadeh, M.; Khakshoor, O.; Russu, W. A.; Nowick, J. S. *J. Am. Chem. Soc.* **2007**, *129*, 2548–2558.

(57) Wishart, D. S.; Sykes, B. D. *Methods Enzymol.* **1994**, *239*, 363–392.

(58) The buried surface area of the solution-state tetramer is 3401 Å², while that of the solid-state tetramer is 2785 Å². (The buried surface area was calculated as the difference between the solvent-accessible surface areas of the individual monomer components and that of the tetramer using the areaimol program in the CCP4 suite.)

(59) Petkova, A. T.; Leapman, R. D.; Guo, Z.; Yau, W.-M.; Mattson, M. P.; Tycko, R. *Science* **2005**, *307*, 262–265.

(60) Paravastu, A. K.; Leapman, R. D.; Yau, W.-M.; Tycko, R. *Proc. Natl. Acad. Sci. U.S.A.* **2008**, *105*, 18349–18354.

(61) Qiang, W.; Yau, W.-M.; Luo, Y.; Mattson, M. P.; Tycko, R. *Proc. Natl. Acad. Sci. U.S.A.* **2012**, *109*, 4443–4448.

(62) Molecular dynamics simulations are an important complement to experimental techniques and can provide valuable insights into the structures of amyloid oligomers at atomic resolution. Polymorphism has been observed in computational studies of $A\beta$ oligomers and mixed oligomers derived from $A\beta$ and tau peptides. For examples, see: (a) Miller, Y.; Ma, B.; Nussinov, R. *Biophys. J.* **2009**, *97*, 1168–1177. (b) Raz, Y.; Miller, Y. *PLoS One* **2013**, *8*, e73303.

(63) Cheng, P.-N.; Pham, J. D.; Nowick, J. S. *J. Am. Chem. Soc.* **2013**, *135*, 5477–5492.